AIAA 80-0327R

Development of a Vortex-Lift Design Procedure and Application to a Slender Maneuver-Wing Configuration

John E. Lamar*
NASA Langley Research Center, Hampton, Va.
Roy T. Schemensky†
General Dynamics Corporation, Ft. Worth, Texas
and
C. Subba Reddy‡
Old Dominion University, Norfolk, Va.

A procedure has been developed to optimize the mean camber surface of a cranked slender wing having leading-edge vortex flow at transonic maneuver conditions using the suction analogy. This type of flow was assumed because it was anticipated that the slenderness of the wing would preclude attached flow at the required lift coefficient. A constraint was imposed in that the camber deflections were to be compatible with a realistic structural-box requirement. The resulting application yielded mean camber shapes which produced effective suction levels equivalent to 77% of the full-planar leading-edge value at the design lift coefficient.

Nomenclature

A	= aspect ratio of wing
a	= fractional chord location where initial chord load changes from constant value to linearly varying value toward zero at trailing edge
C_A	= axial force coefficient
C_D	= drag coefficient
C_L	= lift coefficient
C_m	= pitching moment coefficient about the specified fraction of $\bar{c}$
c	= local chord
$\bar{c}$	= reference chord, mean aerodynamic chord
FVS	= free-vortex sheet
LE	= leading edge
M	= Mach number
QVL	= quasivortex lattice
QVLM	= quasivortex lattice method
QVLM-SF	= quasivortex lattice method coupled with a separated flow representation
SE	= side edge
VLM	= vortex lattice method
VLM-SA	= vortex lattice method coupled with the suction analogy
x/c	= fraction of local chord with respect to local leading edge
z/c	= local elevation relative to the trailing edge normalized by local chord
α	= angle of attack
α_i	= chord incidence angle
ΔC_p	= lifting pressure coefficient, attached flow
$\delta_{LE_{HL}}$	= leading-edge flap deflection angle, positive down, measured normal to the hinge line
$\delta_{TE_{FS}}$	= trailing-edge flap deflection angle, positive down, measured normal to the freestream
λ	= taper ratio, tip chord/root chord
η	= fraction of semispan from the model centerline
τ	= thickness-to-chord ratio

Subscripts

d	= design
0	= measured at $C_L = 0$

Presented as Paper 80-0327 at the AIAA 18th Aerospace Sciences Meeting, Pasadena, Calif., Jan. 14-16, 1980; submitted Feb. 11, 1980; revision received July 28, 1980. This paper is declared a work of the U.S. Government and therefore is in the public domain.

*Aeronautical Research Scientist, FDB, STAD. Associate Fellow AIAA.

†Engineering Specialist, Aerodynamics, Ft. Worth Division. Member AIAA.

‡Assistant Professor, Department of Mechanical Engineering and Mechanics.

Introduction

THERE has been much interest recently in supersonic-cruise fighter aircraft. In concept this aircraft would not only perform the cruise mission at supersonic speeds, but it would also provide transonic-maneuver capabilities similar to the current lightweight fighters. Since this aircraft will most likely be slender in order to provide supersonic efficiency, the transonic-maneuver lift needed will probably be provided by vortex flow. The probable use of vortex lift stems from the fact that maintaining completely attached flow for transonic high-lift conditions on wings with highly swept leading edges is a rather remote possibility. Therefore, the concept of combining vortex lift with a cambered leading edge to develop high lift while recovering some leading-edge thrust and inducing reattached flow in the knee region is an attractive alternative. The problem, of course, is to define the optimum combination of camber shape and vortex strength to minimize the lift-dependent drag.

The design of a slender wing, to be efficient at both supersonic cruise and transonic maneuver, is not easy to accomplish because of the conflicting geometrical requirements brought on by the varying lift coefficients associated with low camber at cruise and large camber during maneuver. One approach to accomplish both requirements would be to design a good supersonic-cruise wing and then to consider how that camber surface could be altered, with maneuver flaps, to give reasonable transonic performance. It may be that at some future date an alternate approach will be considered, in that designs for both requirements would be

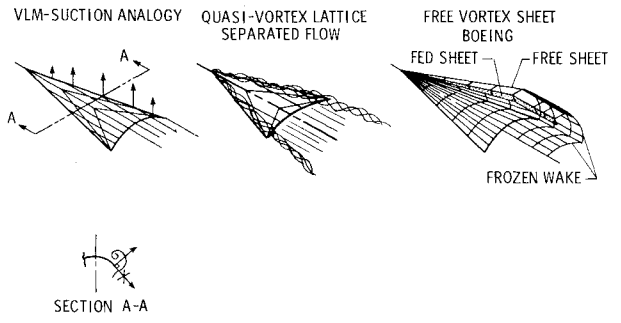

Fig. 1 Vortex-flow aerodynamic representations.

made specifically, then the two merged into a common base with each being achieved through some camber change.

Regardless of the approach used, NASA has been developing analytical tools, both in-house and under contract, that will be of use at these critical design points. The supersonic-cruise attached-flow design methods are in a relatively advanced state of development as indicated in Refs. 1 and 2. On the other hand, the transonic-maneuver design technology for optimizing the warp of slender wings utilizing leading-edge vortex flow is in an earlier stage of development. Apart from solutions obtained with conical flow[3] and those obtained with the vortex lattice method coupled with the suction analogy (VLM-SA) and the free-vortex sheet (FVS) method of Boeing,[4] very little has been published.

With a view toward addressing this technology gap, NASA Langley and General Dynamics, Ft. Worth, undertook a cooperative effort in which both the transonic-maneuver and supersonic-cruise point designs were to be obtained and wind-tunnel models built and tested to help evaluate the methodologies. The configuration chosen for this design study was a cranked highly swept arrow wing which was thin (and sharp edged for the maneuver design). Cranked wings of this type are known to be useful in controlling the aerodynamic-center shift which normally occurs as the speed increases from low to high Mach number.[5] The supersonic design study was reported in Ref. 6, and this paper documents the transonic-maneuver study by detailing the design procedure and its application to this cranked wing. (The aerodynamic methods considered for use in this procedure are actually applicable to subsonic compressible flow rather than transonic flow, since the high sweep of the model leading edges keeps the normal Mach number low.)

In addition, an appendix is provided in which the analytic methods discussed herein are compared with selected swept-wing data sets for an assessment of their respective computational accuracy.

Available Vortex-Flow Analysis Methods

General

Use of a cranked wing for this study pointed up a potential problem in the design process at transonic or high subsonic speeds. That problem was the limited experience in even analyzing planar-cranked wings when vortex flow was present.[7] When this work began, most of the configurations studied previously were planar-swept wings, although some cambered wings had been studied in Ref. 4. Since the cranked wing would most likely have two vortex systems on each semispan, rather than a single one, the design of such a wing represents a jump rather than an incremental step in technology. It was therefore necessary to examine the better available analytical methods with the idea of assessing their ability to analyze the aerodynamic features on various cranked planar wings. Three candidate methods were available to the authors, ranging is simplicity from the VLM-SA to those which model the wing and free-vortex sheet explicitly. The latter include the nine-parameter FVS method[8] developed by Boeing under contract to NASA Langley and the quasivortex-lattice method—separated flow (QVLM-SF)[9] developed by the University of Kansas under grant to NASA Langley. These more exact methods offer the potential for general off-design application. As an example, see Ref. 10.

Description of Aerodynamic Methods

The three analytical methods just mentioned will be briefly discussed herein so that an understanding of their distinct modeling features can be established, in particular with regard to cambered-wing applications. All three satisfy the trailing-edge Kutta condition, but only the FVS and QVLM-SF impose the leading-edge Kutta condition as well. The VLM-SA, on the other hand, approximates the effect of the leading-edge Kutta condition associated with the separated flow by an application of the suction analogy. Figure 1 shows a schematic of the three methods applied to a cambered wing and how the effect of the leading-edge separated flow is represented.

The methods will be discussed in order of the increasing mathematical complexity starting with the VLM-SA.

VLM-SA

As used herein the VLM-SA calculates the leading-edge suction for cambered and twisted wings by using planar boundary conditions in a planar computational plane, then incorporates preliminary corrections to account for the warped surface orientation. After the suction is determined the suction analogy is used with the local surface orientation to arrive at contributions to lift, drag, and pitching moment. This is an extension of the work documented in Ref. 11. This potential-flow suction is obtained along the edge and rotated normal to the surface; from this force the aerodynamic contributions are calculated and added to the potential-flow results.

QVLM-SF

The QVLM-SF procedure[9] uses the QVLM to represent the wing potential flow on a planar-solution surface accounting for camber and twist in the boundary conditions. (The QVLM should be understood to represent the continuous chordwise loads by a series of discrete elements.) To this potential solution is added the separated leading-edge flow modeling of Mehrotra.[9] The modeling encompasses discrete filaments of vorticity that are each composed of multiple straight-line segments which trail from the leading edges. The strength of the filaments and their essentially force-free locations are determined in conjunction with the QVL in the wing solution surface by iteration. The cambered-wing solutions presented herein are among the first documented for this method. (See Ref. 12 for other solutions.)

FVS

The nine-parameter version of the FVS method[8] uses doublet patches of biquadratic variation on the warped-wing surface and on the free sheet. On the fed sheet a quadratic variation is used only along the edge that joins the free sheet. The free- and fed-sheet locations and doublet strengths are also determined by iteration in the presence of the cambered-wing lifting system. Convergence is said to occur when the boundary conditions of no net pressure existing on, or no mass flow through, the free sheet, and the total force normal to the core being zero are satisfied to within a tolerance. Of course, for each solution it is also understood that there is to be no mass flow through the wing. Some applications to cambered/twisted wings have already been made with this method.[13]

Assessment of Methods

For the cranked-wing application, an examination of the three methods reveals that:

1) The QVLM-SF method has restrictions on the wing geometry, i.e., the wing cannot have a cranked leading edge.

2) The FVS method permits only a single-vortex system at the leading edge, not a dual system as envisioned; and the current FVS code has convergence problems for certain groups of cranked wings.

3) Both the QVLM-SF and FVS methods have difficulty modeling the situation where the vortex is small, which occurs when the α is small for a planar wing, or the α is slightly larger than required for the smooth on-flow condition for a cambered wing.

4) The VLM-SA has no geometry restrictions, no convergence or small vortex modeling problems—because the suction analogy approximates the small vortex—but the VLM-SA does not provide for the calculation of the surface pressure distribution with vortex flow. However, the overall forces and moments are well predicted for uncambered wings and appear to be reasonably valid over a lift range for cambered wings near the C_L hypothesized for maneuver design (see Appendix). Hence, the VLM-SA method was selected to use in this design process.

Since the start of this effort, solutions have been obtained on cranked wings using the VLM-SA.[14]

Development of Vortex-Lift Design Procedure and Application to a Cranked Wing

Assumptions

The inherent assumption, basic to the use of the suction analogy for the cambered-wing case, is that the leading-edge vortex system would promote reattached flow near the leading edge. As is well known with the addition of positive camber to a wing, the potential-flow lift will increase at a positive angle of attack. This increase is, however, coupled with a condition in which the flow is more nearly aligned with the leading edge. The "alignment" does two things in the real flow: 1) the leading-edge vortex that is formed near the edge will not only reattach near it, but on a surface which is inclined so as to yield an effective suction or negative drag; and 2) reduces the lift associated with vortex flow. Hence, there exists a dichotomy which must be balanced. A related assumption is that this vortex system will be small, not be shed inboard but extend to the tip, and begin to come into play only on the upper surface as the design C_L is approached. Therefore, the procedure to be followed is based on the flow being not far from the smooth on-flow condition. Hence, an attached-flow solution for smooth on-flow is obtained from a mean camber design method (the VLM technique[15] is employed herein) and used as the initial warped surface.

The procedure outlined next was developed with a particular application in mind. However, a generalization of this procedure can be applied to other configurations.

Design Procedure and Application

The design conditions sought for the joint NASA-General Dynamics cranked wing were $C_{L,d}=0.5$ and $M_d=0.9$. In addition, a rooftop ΔC_p distribution ($a=0.7$) was initially specified along the chord. It should be further noted that the resulting solution for span load from the VLM attached-flow design code was elliptical in keeping with minimum vortex-drag considerations. The method employed uniformly 20 horseshoe vortices chordwise at each of 10 equally spaced spanwise stations on a semispan. This pattern was also used in the VLM-SA code.

The preceding conditions led to the smooth on-flow incidence distribution shown in Fig. 2 for the "wing box." The term wing-box incidence refers to the incidence of the center portion of the wing chord (for this study assumed to lie between 15 and 75% of the local wing chord). The extreme

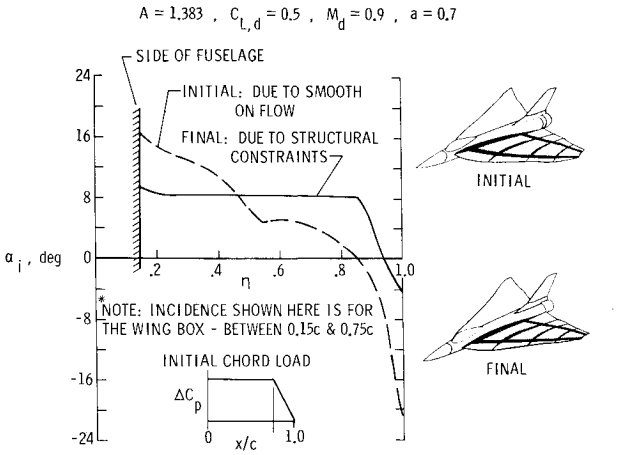

Fig. 2 Incidence distribution for cranked-cambered wing ($A=1.383$, $C_{L,d}=0.5$, $M_d=0.9$, $a=0.7$).

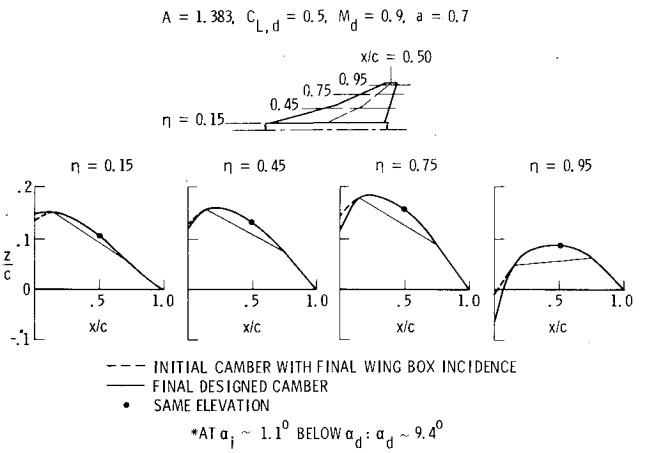

Fig. 3 Cranked-wing mean camber shapes ($A=1.383$, $C_{L,d}=0.5$, $M_d=0.9$, $a=0.7$).

variation of structural box twist, shown in Fig. 2, from the side of the fuselage to the tip required for smooth on-flow would be impractical for any real aircraft configuration. In order to provide a more practical design from structural and aerodynamic standpoints, the final box incidence distribution was used (see Fig. 2). Here the structural box remains at an essentially constant incidence and is twisted only over the outermost 15% of the semispan.

Lines connecting the wing-box leading and trailing edges at four different span stations for the final incidence are shown in Fig. 3. Though the z/c and x/c scales are different, the relative incidence variation across the span is discernable. Associated with each of these lines, as well as the other stations across the wing, is the initial smooth on-flow camber rotated by the difference of the two α_i curves in Fig. 2 and passing through the trailing edge. This combination of incidence and camber was then analyzed using the VLM-SA procedure to determine lift, drag, and the strength of the suction force along the leading edge and to provide a reference for successive modifications. The camber ahead of the wing box (15% chord) was then represented by five equal semispan cambered leading-edge flap segments whose deflection angles were adjusted parametrically while monitoring the VLM-SA drag level. Even though these levels were optimistic, they were considered reliable in estimating the proper trend of lowering drag with flap deflection angle. After a set of angles was obtained about the 15% chord line which produced a minimum drag value, the resulting camber was smoothed and the process was repeated about the 2.5%

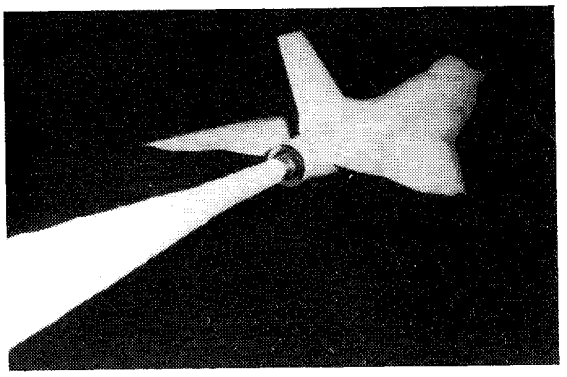

Fig. 4 Designed wing on fuselage, 3/4 rear view.

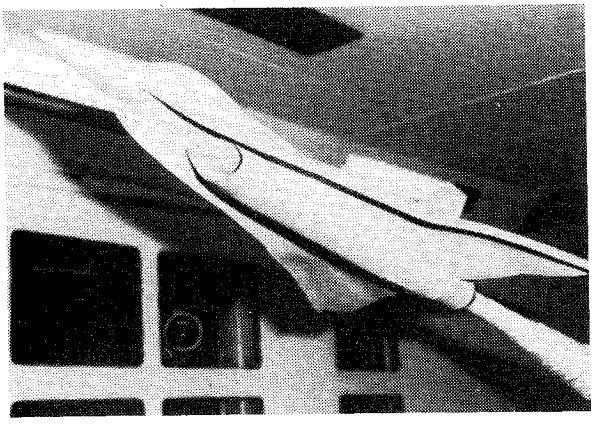

Fig. 5 Designed wing on fuselage, 3/4 front view.

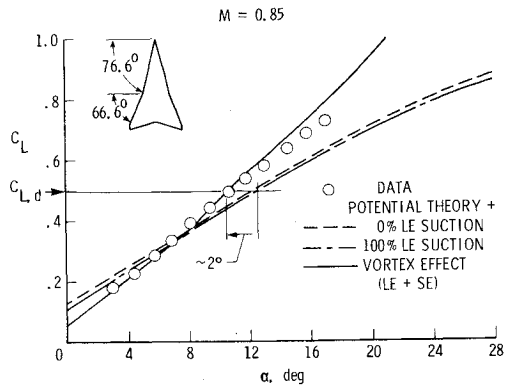

Fig. 6 Transonically cambered-wing lift characteristics ($M = 0.85$).

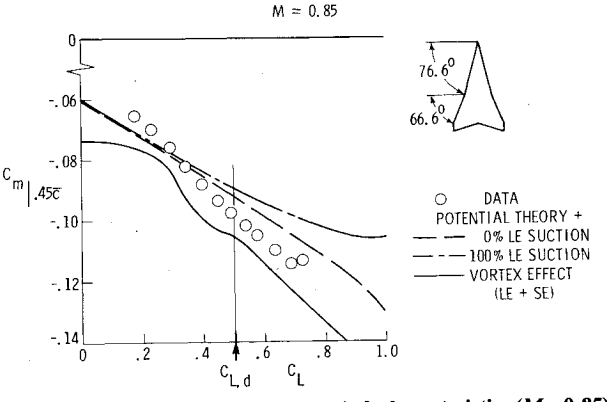

Fig. 7 Transonically cambered-wing pitch characteristics ($M = 0.85$).

chord line. These smoothed camber lines are shown in Fig. 3 and labeled the final designed camber. It should be noted that the final camber shapes are changed in the direction of the initial incidence distribution (shown in Fig. 2).

In order to put this camber on the wing, two things were done. The first was to shift the local camber distribution vertically to provide a constant elevation along the wing midchord. The second was to match the fuselage incidence to the final inboard wing incidence to provide an even wing-fuselage juncture. (Note that the $C_{L,d}$ occurs at an α of -9.4 deg.) Photographs of the designed wing mounted on an existing fuselage appear as Figs. 4 and 5.

For the final camber, the VLM-SA code indicates that $C_{L,d}$ occurs at a wing α slightly larger than required for smooth on-flow all across the span. If the flow features which are indicated are largely realized, then this should enable a large amount of the available leading-edge suction to be recovered at the design point.

Data obtained for the cranked wing just designed are compared in the next section with theory, and an assessment of the design procedure is made therein.

Analysis of Cranked-Wing Data and Assessment of Design Procedure

Analysis of Data

This cranked-wing model was tested at $M = 0.85$ rather than at $M_d = 0.90$ because of power limitations in the Langley 7×10 ft High-Speed Tunnel, and the test Reynolds number was 7.5×10^6 based on $\bar{c}$. The data are presented in Figs. 6-11 and Fig. 14. In Figs. 6 and 7 there are three theoretical curves included which are determined in a single run of the VLM-SA code. Each contains the potential-flow contribution from the VLM solution but in each the leading-edge suction contribution is treated differently. One solution omits it, another includes it directly, and a third rotates it normal to the surface at the leading edge in accordance with the suction analogy, before computing the contributions. After the data analysis is completed an assessment of the design procedure is made.

Lift

The lift comparison presented in Fig. 6 shows that the VLM-SA method (solid curve), obtained by combining the potential-flow results with the vortex lift from the leading and side edges, predicts the measured lift well over an α range of 3-12 deg. Above $\alpha = 12$ deg there is a loss in the amount of vortex lift realized, partially due to the lack of flow reattachment in the region of the wing-tip trailing edge as a consequence of the real flow having insufficient chord there to permit the finite-sized vortex to develop reattached flow and full lift.[7] (For wings with trailing-edge notching this lift loss is increased.) Regarding the comparison with the solution from potential theory plus 100% leading-edge suction, it is apparent that up to about $\alpha = 8$ deg the effect of the vortex flow is to reduce the lift, indicative of reattachment on the lower surface; whereas, above $\alpha = 8$ deg the effect of the vortex is to increase lift, indicative of reattachment on the upper surface. Another interesting feature of obtaining $C_{L,d}(=0.5)$ with vortex flow is that in comparison with the potential-flow solution for this same cambered wing an angle of attack of about 2 deg less is required. Of course, it is realized that this wing was not designed to reach $C_{L,d}$ with potential flow. Still it is interesting to realize that theoretically there is an angle-of-attack reduction possible if vortex flow is present on the slender cambered wing, especially since vortices would tend to form naturally on such a wing.

With regard to the 0% suction with no vortex lift and the 100% leading-edge suction solutions, it is noteworthy that the presence of the potential flow leading-edge suction on the highly cambered leading edge actually reduces the C_L over the α range shown. This is, of course, due to the edge force acting tangentially to the highly cambered leading edge, thereby creating a negative lift force.

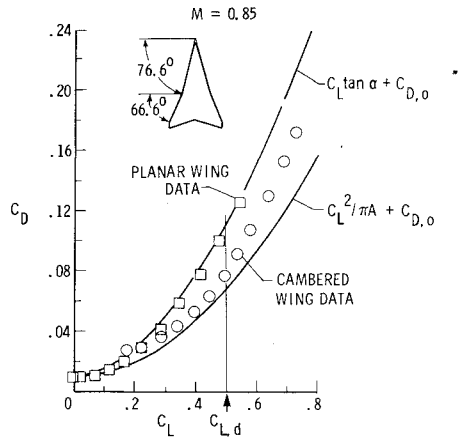

Fig. 8 Transonic maneuver drag efficiency for wing designed to have vortex flow ($M = 0.85$).

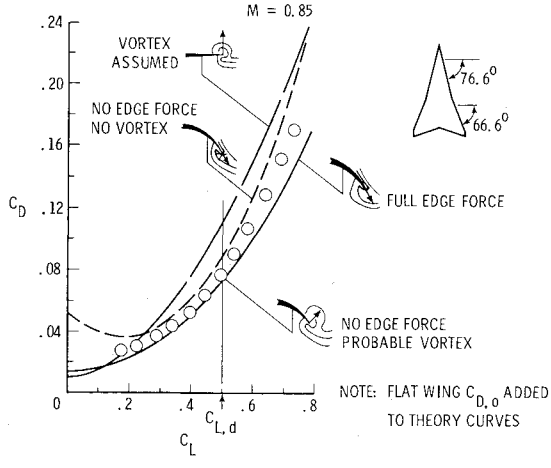

Fig. 9 Edge force recovery on transonically cambered wing ($M = 0.85$).

Pitching Moment

The pitching moment characteristics are shown in Fig. 7 on a plot with a broken and expanded scale. As pointed out previously the VLM-SA does not generate a load distribution consistent with the actual three-dimensional flow, hence some differences with the C_m vs C_L theory and data are expected. A comparison made between the theoretical curves and the data shows that except for a $C_{m,0}$ difference the curve which includes vortex lift estimates the data and slope reasonably well for $C_L > 0.25$ and best of all for $C_L > 0.5$. The other two theoretical curves also display $C_{m,0}$ differences with the data and, in general, less stability for $C_L > 0.25$ than do the data or the curve which includes the vortex lift. Furthermore, it should be noted that the maximum spread between the data and any of the theoretical curves, especially the solid one, is about 0.01 for the C_L range of the data.

The unusual shape of the VLM-SA curve is due to the rotated sectional edge force not acting on the same side of the wing all across the span for $0 \leq C_L \leq 0.50$. For C_L values ≤ 0.25 all the rotated edge forces act on the lower surface and for C_L values ≥ 0.50 all the rotated edge forces act on the upper surface. In between these two C_L values the rotated edge forces begin to change from the bottom to the top and from the tip inboard as α increases.

Performance

Drag Polars

Figures 8-11 present the drag data and other data to aid in its interpretation. For example, Fig. 8 shows both the planar

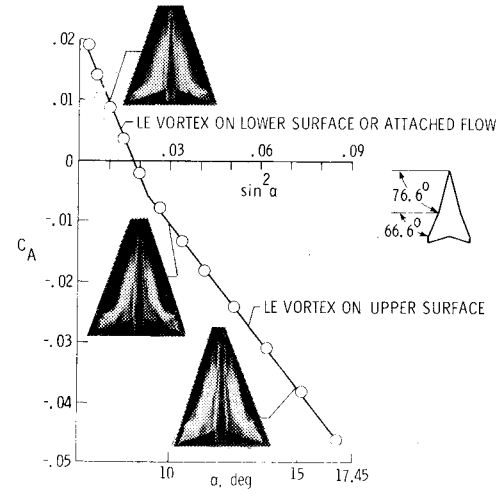

Fig. 10 Effect of flow type on transonically cambered wing ($M = 0.85$).

and cambered wing drag polars in comparison with two theoretical curves. Over most of the C_L range the planar-wing data follow the upper or zero edge-force curve as expected. The cambered-wing data are generally much lower than the planar-wing data and approach the lower bound polar in the C_L range of about 0.35-0.45, even though the wing is thin (maximum $\tau = 3.2\%$) and the leading edge is sharp. Furthermore, at the design C_L the data reach a level equivalent to 77% of full leading-edge suction. This large value of equivalent suction is remarkable for such a slender wing, particularly at this high Mach number maneuver condition. The data further show that a larger fraction of leading-edge suction is realized at $C_L = 0.4$, indicating that the wing mean camber surface has not been fully optimized at the design C_L.

Figure 9 displays the same cambered-wing drag data but here in place of the planar-wing lower bound polar are two attached flow polars obtained from the VLM-SA code. One is for full edge force, 100% leading-edge suction and the other for no edge force, 0% leading-edge suction. It is well known that a planar wing of the same shape will have more edge force than a corresponding cambered wing under the same conditions, because a portion of the suction available on the cambered wing is distributed chordwise over the surface. Thus, the figure shows that the displacement between the full- and no-edge-force curves to be smaller than for the planar wing. Further, the data are quite close to the full-edge-force curve for C_L values equal to or less than $C_{L,d}$. This is in keeping with the original idea of being at an angle of attack slightly above that for smooth on-flow, in that at smooth on-flow full suction is realized but is distributed over the cambered surface. In terms of the suction available, this cambered wing achieves a level of effective leading-edge suction of about 67%.

Axial Force

Another way to establish when flow changes occur on the wing, beyond examining the C_L vs α curve, is to examine the axial force, since it is a sensitive measure of the edge flow. Figure 10 shows the axial-force coefficient variation for the cranked cambered wing as a function of $\sin^2\alpha$, because both the edge-force and vortex-flow terms have this dependency. It is interesting to note the sharp change in the C_A variation near $\alpha \sim 9$ deg, because at this same α the lift data of Fig. 6 show a rapid change.

The faired straight lines in Fig. 10 have associated with them labels describing the types of flow which are hypothesized to be present. From the inserts of planview oil flow photographs, it is clear that at both $\alpha = 5$ and 10 deg the flow on the upper surface appears to be attached even though

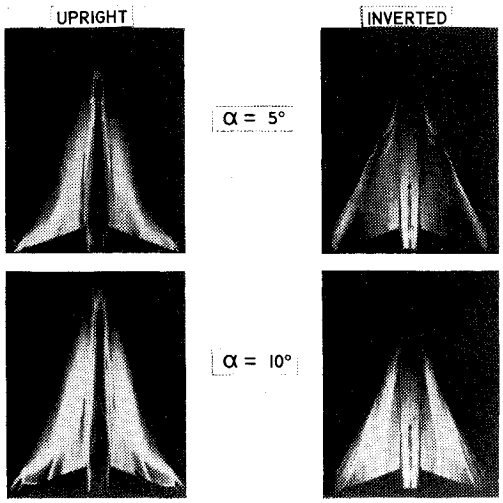

Fig. 11 Plan view of oil flow (cranked-cambered wing, $M = 0.7$).

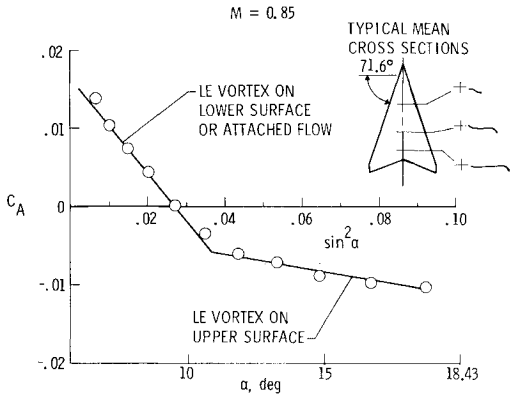

Fig. 12 Effect of flow type on cambered wing ($M = 0.85$).

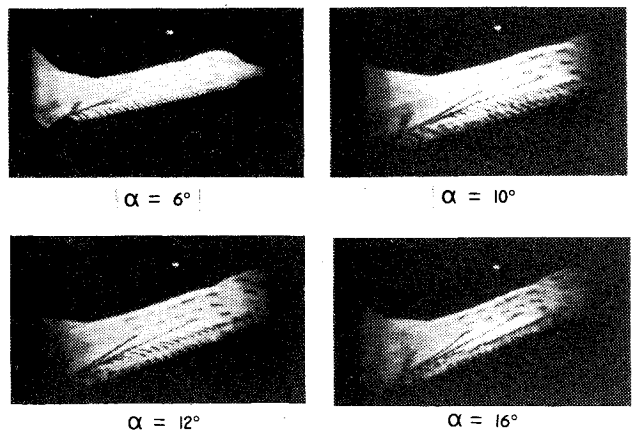

Fig. 13 Tuft patterns on swept-cambered wing having leading-edge vortex flow ($M = 0.85$).

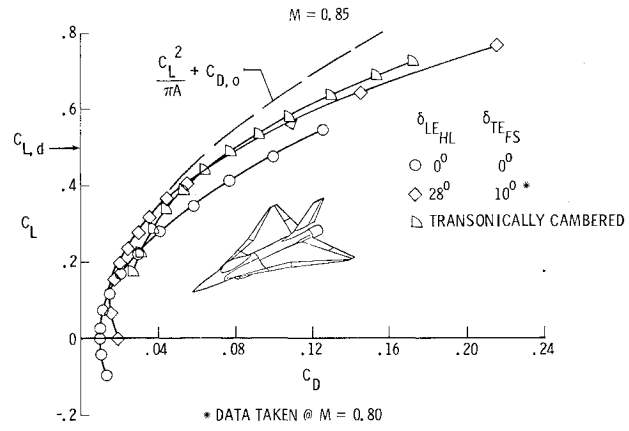

Fig. 14 Drag polars for best flapped wing and transonically cambered wing ($M = 0.85$).

the C_A curve shows that some change in the data has occurred. It needs to be remembered here that, since this leading edge is highly cambered, the flow at the edge cannot easily be seen from the top. At $\alpha = 15$ deg there is a definite indication of vortex activity on the upper surface, which means that the vortex system has just formed or become strong enough to be noticeable.

Oil Flow

To obtain a clearer understanding of what happens with increasing α, top and bottom available oil flow photographs (labeled upright and inverted, respectively) of this wing at $M = 0.70$ are presented in Fig. 11. These photos at $\alpha = 5$ and 10 deg are very instructive in that while there appear to be no major changes in the flow on the top surface near the leading edge (in comparison to one another or to those at $M = 0.85$), the bottom surface shows that there is a reattached vortex flow present at $\alpha = 5$ deg but not at 10 deg. Hence, with the wing being thin and the edge sharp, there are only three possible locations for the leading-edge vortex system at $\alpha = 10$ deg. It is either: 1) present on the lower surface but not visible due to the severity of the leading-edge camber, 2) not present because of smooth on-flow, or 3) present on the upper surface but too small to be noticed. However, the data of Fig. 10 indicate that something happens to the flow type at $\alpha \sim 9$ deg and with increasing α the flow type does not change again. Thus, with the wing being slender, the structure of the flow being the same at $M = 0.70$ and 0.85, and the upright planview photo appearing similar, it is concluded that the hypothesized flow is correct and that the leading-edge vortex system begins to act on the upper surface at values of $\alpha \sim 9$ deg.

Related Axial Force/Tuft Study

As corroborative evidence of a qualitative nature, data are presented here for a cambered wing that is similar in aspect ratio, area, and sweep. This wing was also tested in the Langley 7 × 10 ft High-Speed Tunnel as part of the slender-wing research program. The C_A data at $M = 0.85$ is shown in Fig. 12 for this cropped arrow wing, and sideview tuft photographs for the wing at critical values of α are shown in Fig. 13. These C_A data show a less linear variation with $\sin^2\alpha$ than do those of Fig. 10; however, with α reaching 10 deg a change in the flow types does become more apparent. The tuft photographs of Fig. 13 show that: at $\alpha = 6$ deg the upper surface exhibits attached flow; at $\alpha = 10$ deg portions of the leading edge begin to show separated flow with reattachment; at $\alpha = 12$ deg a leading-edge vortex must be present all along the edge with the reattachment occurring forward of the shoulder; and at $\alpha = 16$ deg the reattachment line of the vortex system has already crossed over the shoulder.

Hence, the C_A vs $\sin^2\alpha$ graphs provide a good indication of the flow type and which surface is involved. Graphs of this type have, of course, been used by others, especially with regard to defining buffet onset from wind-tunnel data.

Flapped Planar Cranked-Wing Drag-Polar

During the test of the cranked-cambered wing, a planar wing with full-span leading- and trailing-edge flaps was tested to determine if there were flap combinations which would yield the same level of performance as the designed wing. The hinge lines for the flaps are shown on the wing in Fig. 14. Deflection angles about these hinge lines of 28 and 56 deg down at the leading edge (measured normal to the hinge line)

and 0 and 10 deg down at the trailing edge (measured normal to the freestream) were used. The 56 deg deflection was chosen because it best represented an average of the leading-edge camber across the span of the designed wing. All four combinations of deflections were tested but the one which produced the best polar was singled out for presentation with the cambered-wing drag data in Fig. 14.

Figure 14 shows that the flat wing deflected $\delta_{LE_{HL}} = 28$ deg and $\delta_{TE_{FS}} = 10$ deg had a better polar than the designed wing up to $C_L \sim 0.4$, however, for large C_L values the designed wing was better. Since only four combinations of flaps were tested, it is likely that the optimum combination has yet to be found for this cranked wing at $M = 0.85$.

Design Procedure Assessment

It is encouraging that the VLM-SA method could be coupled with structural constraints and still produce effective leading-edge suction levels using vortex-flow aerodynamics that are compatible with the lower bound for C_D. This is especially true because of the complexity associated with the ability of the cranked wing to produce two, rather than one, leading-edge vortices. Furthermore, the lift, stability, and $C_{m|0.45\bar{c}}$ levels were well estimated. All the preceding resulted from the leading-edge vortex system being kept small and forming on the upper surface at an α slightly below that required for $C_{L,d}$, in keeping with the assumption of this effort.

There is room for improvement in the method employed, in that slightly higher values of effective leading-edge suction were realized at C_L values just below $C_{L,d}$. Furthermore, there is a tip stall problem which exists at even $\alpha = 5$ deg. The tip and trailing-edge region camber need to be refined to promote better flow.

Lastly, it is possible to achieve comparable drag polars as the wing designed herein, by using simple leading- and trailing-edge hinged flaps mounted on a planar-cranked wing. The flapped wing that was best had an even better polar than the designed wing up to $C_L = 0.4$. However, for $C_L \geq C_{L,d}$ the smoothly contoured designed wing was best.

Conclusions

From the development of a procedure to design the mean camber surface of a slender cranked wing, taking into account the vortex-flow characteristics under transonic maneuver conditions, and its application, the following conclusions can be drawn: 1) the vortex lattice method coupled with the suction analogy can be a useful means of obtaining mean camber shapes for wings having structural constraints and efficient leading-edge vortex flows, because the assumption of a small vortex close to the leading edge can be realized near the design lift coefficient; 2) at the design lift coefficient a level of effective or recovered leading-edge suction of 77% was reached when compared with the reference planar solutions; and 3) the tip and trailing-edge region cambers need special attention to avoid poor flow.

Appendix: Analysis of Simple Swept Cambered Wings

As part of the present study, the analytical capability of the three aerodynamic theories which include leading-edge vortex flow assumptions, described in the body of the paper, were investigated for several simple swept-cambered wings. Three sets of data on swept-cambered wings were selected for comparison with the VLM-SA, QVLM-SF, and FVS methods in this section. Two sets are for delta wings, Squire's wings-2 and -7,[16] and are shown in Figs. A1 and A2. The associated camber is conical and analytically prescribed and is shown there along with the data. The other data set is from recent tests of a cropped-arrow wing tested in the Langley 7×10 ft High-Speed Tunnel and is shown in Fig. A3. This wing is highly cambered both chordwise and spanwise, especially near the leading edge as can be seen from the typical mean cross sections. All theory curves shown for C_D have the planar wing $C_{D,0}$ included. Table A1 gives the computational pattern for each method as applied to each wing.

Deltas

Figure A1 shows that the C_L and C_D data for Squire's wing-2 are reasonably well estimated by all three methods, but the $C_{m|0.25\bar{c}}$ data are better estimated by the QVLM-SF and the FVS methods for C_L values above 0.5. This figure also points up some of the differences that exist between the three methods for $\alpha \geq 25$ deg. In particular, the VLM-SA method generally estimates more C_L, less C_D, and more nose-down C_m than the others. These features are not new. They have been explained in Ref. 7 and reiterated partially in the discussion of designed wing lift. Although the suction analogy accounts for vortex strength it makes no accounting for vortex size with change in α, assuming instead that the vortex is always small and located at the wing leading edge. Furthermore, just as the QVLM-SF estimates C_m at higher values of C_L better than the FVS method for this conically cambered wing, so the QVLM-SF also yields the best agreement of the three with C_m data for planar deltas.[9]

Figure A2 shows Squire's wing-7 which is representative of a planar wing with a smoothly attached and cambered leading-edge flap at a relatively high deflection angle. The comparison of the theories with the data show that the estimates from the FVS to be best over the C_L range and is followed, in order of accuracy, by those from the VLM-SA and the QVLM-SF methods. Solutions for the FVS method were obtained at $\alpha = 10$-30 deg in 5 deg increments, and those for the QVLM-SF method were calculated at $\alpha = 10$-35 deg, also in 5 deg increments. However, converged solutions were not obtained at $\alpha = 15$ and 25 deg for the QVLM-SF method, so a curve is faired only through the converged data points. The reason for this unusual occurrence, i.e., solutions converging at certain α and not at those in between, is not completely understood but must be related to the variation of the strength and location of the free filaments with the iteration cycle. Evidently, for these angles certain filaments

Table A1 Panel layout on wings for simple swept-cambered wings

Method	Direction	Squire's wing-2	Squire's wing-7	Cropped arrow
VLM-SA	Chordwise	6	8	20
	Spanwise	24	22	10
QVLM-SF	Chordwise	6	6	6
	Spanwise	9	9	8
FVS	Chordwise	8	8	--
	Spanwise	6	9	--

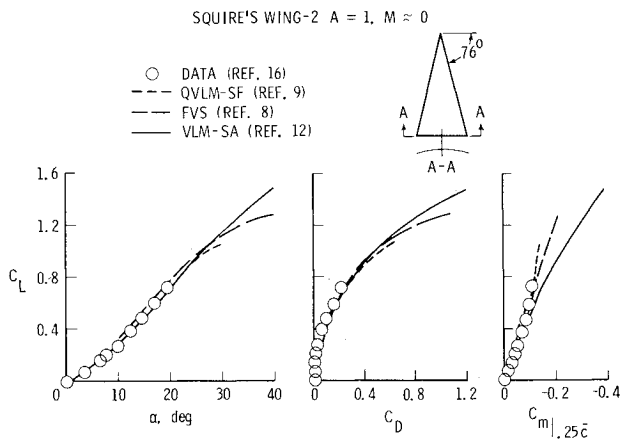

Fig. A1 Longitudinal aerodynamic results for spanwise cambered-delta wing (Squire's wing-2, $A = 1$, $M \sim 0$).

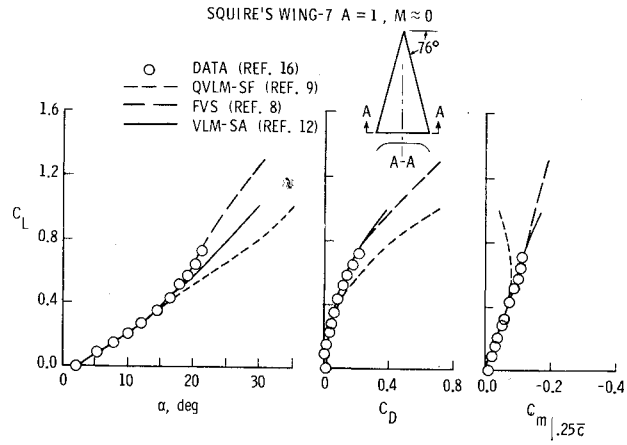

Fig. A2 Longitudinal aerodynamic results for spanwise cambered-delta wing (Squire's wing-7, $A = 1, M \sim 0$).

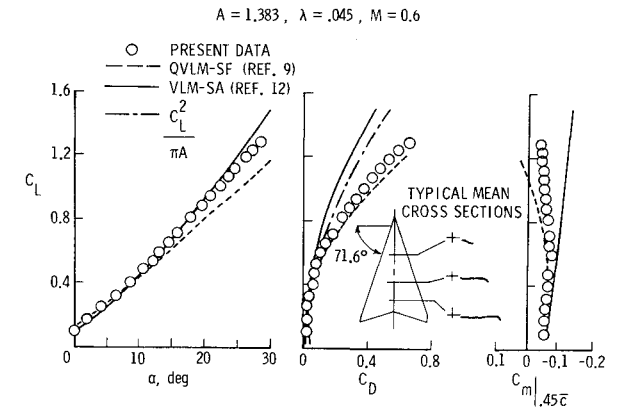

Fig. A3 Longitudinal aerodynamic results for cambered wing ($A = 1.383$, $\lambda = 0.045$, $M = 0.6$).

are tending to be collocated and during the resulting iterations the filament movements are not being "damped out" to convergence.

Cropped Arrow

Theoretical results and data for the highly cambered cropped-arrow wing are shown in Fig. A3. The data were taken with the wing mounted on a fighter-type fuselage such that the wing covered all but a small portion near the nose. Solutions were not available with the FVS method, and therefore comparisons are made only with the other two. The theoretical C_L results show both the VLM-SA and QVLM-SF to estimate the data reasonably well. However, for C_D and $C_{m|0.45\bar{c}}$ the data are better estimated by the QVLM-SF method above $C_L = 0.5$ for C_D and $C_L = 0.6$ for $C_{m|0.45\bar{c}}$. Note on the drag plot that the planar lower bound curve is added for reference. With respect to it, the data and the QVLM-SF results show that they are quite far from achieving suction recovery equivalent to full leading-edge suction at the higher C_L values. On the other hand, the VLM-SA results are seen to be optimistic for C_L values larger than ~ 0.4 and the differences between the two curves grow at a slow rate as C_L increases. These optimistic levels can be attributed, in part, to the assumption mentioned previously in applying the suction analogy to the cambered wing, which results in the rotated edge force remaining concentrated along the edge regardless of the α.

Overall Results

From the detailed evaluation of the three theories for these three wings, it is clear that for $C_L \sim 0.5$ any of the methods which converge will yield about the same global results for highly swept cambered wings. This lift coefficient appears adequate for a slender wing since it would have a lower design wing loading and can use a lower design C_L for maneuver than the current group of maneuvering fighters while maintaining the same level of maneuverability. In particular, for the cranked-wing configuration studied herein, a C_L value of 0.5 is sufficient to provide the same level of maneuverability as the current class of lightweight fighters.

Regarding the VLM-SA method, it was determined that the drag levels estimated in the design C_L range may be slightly optimistic. However, this method estimates well the camber effect as illustrated by its prediction of the angle for zero lift, a condition in which the vortex flow and reattachment are most likely occurring on the lower surface.

Acknowledgments

Steve Hadley of General Dynamics, Ft. Worth, made major contributions to the development of the vortex-lift design procedure. Edward Tinoco of Boeing Aerospace Company obtained some of the first solutions at high angles of attack with the FVS method for Squire's wing-7.

References

[1] Miller, D.S. and Middleton, W.D., "An Integrated System for the Aerodynamic Design and Analysis of Supersonic Aircraft," *Aerodynamic Analyses Requiring Advanced Computers,* NASA SP-347, March 1975, pp. 1049-1065.

[2] Miller, D.S., Carlson, H.W., and Middleton, W.D., "A Linearized Theory Method of Constrained Optimization for Supersonic Cruise Wing Design," *Proceedings of SCAR Conference,* NASA CP-001, Nov. 1976, pp. 9-24.

[3] Nangia, R.K., "On Slender Wings with Leading Edge Cambers," *Symposium on High Angle of Attack Aerodynamics,* AGARD-CP-247, Jan. 1979.

[4] Lamar, J.E., "Subsonic Vortex Flow Design Study for Slender Wings," *Journal of Aircraft,* Vol. 15, Sept. 1978, pp. 611-617.

[5] Lamar, J.E. and Alford, W.J. Jr., "Aerodynamic-Center Considerations of Wings and Wing-Body Combinations," NASA TN D-3581, Oct. 1966.

[6] Miller, D.S. and Schemensky, R.T., "Design Study Results of a Supersonic Cruise Fighter Wing," AIAA Paper 79-0062, New Orleans, La., Jan. 15-17, 1979.

[7] Polhamus, E.C., "Prediction of Vortex-Lift Characteristics by a Leading-Edge Suction Analogy," *Journal of Aircraft,* Vol. 8, April 1971, pp. 193-199.

[8] Johnson, F.T., Lu, P., Tinoco, E.N., and Epton, M.A., "An Improved Panel Method for the Solution of Three-Dimensional Leading Edge Vortex Flows-Vol. I. Theory Document," NASA CR 159173, 1979.

[9] Mehrotra, S.C. and Lan, C.E., "A Theoretical Investigation of the Aerodynamics of Low-Aspect-Ratio Wings with Partial Leading-Edge Separation," NASA CR 145304, Jan. 1978.

[10] Tinoco, E.N. and Yoshihara, H., "Subcritical Drag Minimization for Highly Swept Wings with Leading Edge Vortices," *Symposium of High Angle of Attack Aerodynamics,* AGARD-CP-247, Jan. 1979.

[11] Lamar, J.E. and Gloss, B.B., "Subsonic Aerodynamic Characteristics of Interacting Lifting Surfaces with Separated Flow Around Sharp Edges Predicted by a Vortex-Lattice Method," NASA TN D-7921, Sept. 1975.

[12] Reddy, C.S., Lin, T.H., and Hsu, C.T., "Numerical Investigation of Aerodynamic Characteristics of Wings with Separation—Induced Flows," Old Dominion University Research Foundation, Final Rept. NAS 1-14193, Task 48, Oct. 1978.

[13] Johnson, F.T. and Tinoco, E.N., "Recent Advances in the Solution of Three-Dimensional Flows Over Wings With Leading Edge Vortex Separation," AIAA Paper 79-0282, New Orleans, La., Jan. 15-17, 1979.

[14] Lamar, J.E., "Analysis and Design of Strake-Wing Configurations," *Journal of Aircraft,* Vol. 17, Jan. 1980, pp. 20-27.

[15] Lamar, J.E., "A Vortex-Lattice Method for the Mean Camber Shapes of Trimmed Noncoplanar Planforms with Minimum Vortex Drag," NASA TN D-8090, June 1976.

[16] Squire, L.C., "Camber Effects on the Non-Linear Lift of Slender Wings With Sharp Leading Edges," Aeronautical Research Council, CP 924, 1967.